

Infrared Thermography Measurements of Window Thermal Test Specimen

Surface Temperatures

Brent T. Griffith *ASHRAE Member*, Howdy Goudey, and
Dariush Arasteh P.E. *ASHRAE Member*

Building Technologies Program
Environment Energy Technologies Division
Lawrence Berkeley National Laboratory
University of California
Berkeley CA 94720 USA

August 2, 2001

This work was supported by the Assistant Secretary for Energy Efficiency and Renewable Energy, Office of Building Technology, State and Community Programs, Office of Building Systems of the U.S. Department of Energy under Contract No. DE-AC03-76SF00098.

Surface Temperatures of Window Specimens: Infrared Thermography Laboratory Measurements

Brent T. Griffith¹, Howdy Goudey, and Dariush Arasteh

ABSTRACT

Temperature distribution data are presented for the warm-side surface of three different window specimens. The specimens were placed between warm and cold environmental chambers that were operated in steady state at two different standard design conditions for winter heating. The American Society of Heating, Refrigerating and Air-Conditioning Engineers (ASHRAE) temperature conditions were 21.1°C (70°F) and -17.8°C (0°F) on the warm and cold sides, respectively. The International Standards Organization (ISO) temperature conditions were 20.0°C (68.0°F) and 0.0°C (32.0°F) on the warm and cold sides, respectively. Surface temperature maps were compiled using an infrared thermographic system with an external referencing technique, a traversing point infrared thermometer and thermocouples. The infrared techniques allow detailed, non-intrusive mapping of surface temperatures. Surface temperature data are plotted for the vertical distribution along the centerline of the window specimen. This paper is part of larger round-robin collaborative effort that studied this same set of window specimens. These studies were conducted to improve and check the accuracy of computer simulations for predicting the condensation resistance of window products. Data collected for a Calibrated

¹ B.T. Griffith is Staff Research Associate, H. Goudey is Scientific Engineering Associate, and D. Arasteh is Staff Scientist at Lawrence Berkeley National Laboratory, Berkeley, CA.

Transfer Standard showed that convective effects outside the window gap are important for predicting surface temperatures.

INTRODUCTION

The condensation performance of a fenestration product is strongly influenced by the temperatures on the warm inside surface when outdoor conditions are cold. Future efforts to rate and label the relative condensation resistance of windows are expected to rely on computer simulations. Although current window performance rating focuses on U-factor for which accurate surface temperature distributions are not necessary, computer models to rank window condensation characteristics will be more accurate if accurate prediction of window surface temperatures is possible. The development and validation of such computer models can benefit from detailed experimental data on surface temperatures of specimens under standard environmental conditions.

An earlier collaborative research project studied identical sets of insulated glazing units (IGUs) (Sullivan et. al. 1996). The project focused on comparing results for the vertical distribution of surface temperatures down the center lines of IGUs. Two laboratories measured specimens using infrared thermography (Elmahdy 1996, Griffith et al.1996). Two separate groups simulated heat flow using conjugate Computational Fluid Dynamics modeling tools (de Abreu et al. 1996, Zhao et al. 1996). The success of this project led to the current research on entire window assemblies rather than just glazings.

This paper presents data on the distribution of surface temperatures for three window test specimens that were subjected to winter heating conditions in a laboratory. The specimens

include a calibrated transfer standard (CTS), a clear wood casement window, and the same wood casement with a low-emittance (low-E) glazing system. The specimens were mounted between warm and cold environmental chambers and measured under two different, steady-state conditions for winter heating. The data were gathered using infrared (IR) thermography, which is a non-destructive method of mapping surface temperatures by measuring the thermal radiation emanating from an object. In addition to using an imaging IR scanner, we also investigated the potential for using a point IR thermometer in conjunction with a traversing system to gather such temperature maps. This paper is closely associated with papers by other authors that measured or modeled the same set of specimens in a blind study [[insert references when available]].

SPECIMENS

Table 1 lists the thermal test specimens and describes the glazing system and specimen size. Figure 1 shows the geometry and mounting of the first specimen, the CTS (ASTM 1995). The CTS was constructed with twelve pairs of thermocouple providing four measurements along the centerline. Figure 2 diagrams the geometry and mounting of the second and third specimens, which are fixed wood casements. The specimens were mounted in a foam surround panel with 3.5 mm skins of acrylonitrile-butadiene-styrene (ABS) sheet plastic and had an overall thickness of 152 mm. The CTS was mounted 25 mm from the surround panel cold-side surface. The clear and low-E windows were mounted with their cold-side surfaces flush with the cold-side surface of the surround panel. The specimens were sealed with vinyl tape on both sides; the tape extended 12.7 mm onto the specimen at these joints. Location markers, consisting of 50 by 3 mm strips of aluminum tape, were mounted on the specimens for later use in identifying geometry and spatial locations in the thermographic image data. Four thermocouples were mounted on the

specimen centerline in the following locations: center of glass, 100 mm from the sill sightline, 10 mm from the sill sightline, and, for the CTS, on the surround panel opening at 60 mm from the sightline; for the clear and low-E windows, the fourth thermocouple was located on the window frame 20 mm from the sill sightline. Thermocouples were mounted using 0.05 mm thick vinyl tape; more than 75 mm of wire was in good contact with the specimen.

Table 1. Thermal Test Specimens

Specimen ID	Type	Frame Material	Glazing Configuration	Overall Size W x H (mm) (ft. inch)
CTS	Calibrated Transfer Standard	N/A	≈12.5 mm foam 12 pairs of thermocouples	610 x 914 (2' 0" x 3' 0")
Clear	Fixed Casement	Wood	Dual, air-filled Clear-Clear 16.5-mm gap	610 x 914 (2' 0" x 3' 0")
Low-E	Fixed Casement	Wood	Dual, air-filled Clear-Low-E 16.5-mm gap	610 x 914 (2' 0" x 3' 0")

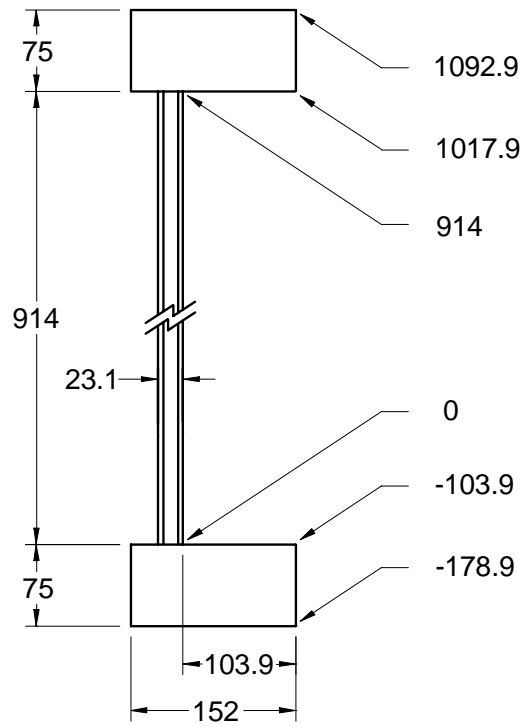


Figure 1. CTS and Mounting Showing Accumulated Distances in mm

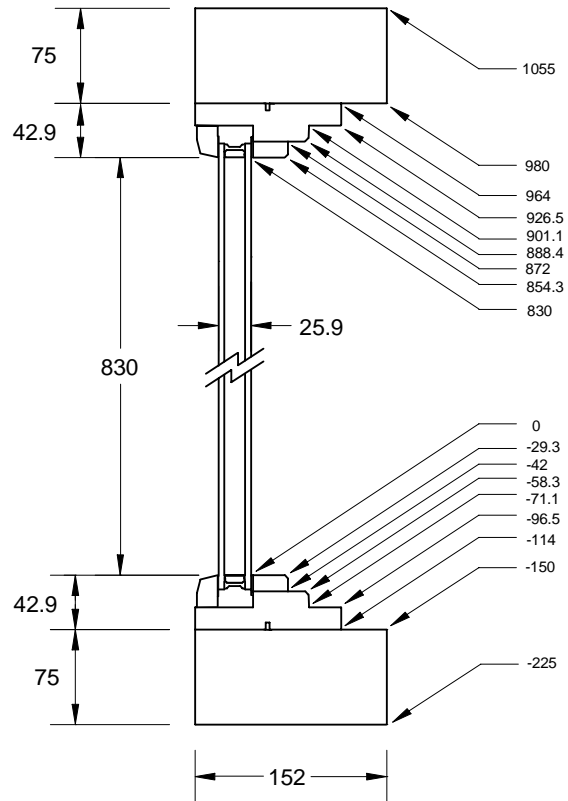


Figure 2. Wood Casement Window Geometry with Surround Panel and Accumulated Distances in mm

THERMAL TEST CHAMBERS

Two environmental chambers with different air temperatures -- a climate chamber and a thermography chamber -- were used to generate steady-state heat flow across the test specimens in the infrared thermography laboratory (IRLab). Infrared thermographic measurements take place in the thermography chamber. This chamber is controlled to provide stable room temperature with nominally still air. The climate chamber simulates cold weather on the outside surface of a building component during the heating season. The laboratory configuration differs from the one used for conventional hot boxes in that the chambers are smaller and have a different warm-side configuration, and no serious precautions were made to restrict heat flow

through the walls of the warm-side chamber. The test conditions were chosen to match the design conditions recommended for rating the thermal performance of fenestration products by either the American Society of Heating Refrigerating and Air-Conditioning Engineers (ASHRAE) or by the International Standards Organization (ISO). ASHRAE winter design conditions specify cold-side temperature conditions of -17.8°C and warm-side conditions of 21.1°C . ISO conditions specify cold-side temperature conditions of 0.0°C and warm-side conditions of 20.0°C . The thermal chambers used in the IRLab are discussed below and shown in Figure 3.

Climate Chamber

The climate chamber used at the IRLab directs airflow upwards and parallel to the test specimen through a plenum with a (baffle) depth of 10 cm from the plane of the specimen surround panel's surface. Air leaving the blower circulates upward across the specimen, is forced through the cooling coil, passes controlled strip heaters, and then returns to the blower. Absolute air speed near the center of the specimen for these measurements was between 1.9 and 3.6 m/s, depending on the moisture loading of the cooling coil (duration of operation). Three separate zones (across the width of the plenum) are controlled with instruments capable of $\pm 0.05^{\circ}\text{C}$ accuracy. During testing of the first specimen, the CTS, the overall surface conductance was measured at $30 \pm 2 \text{ W/m}^2\cdot\text{K}$ for the ASHRAE conditions and $24 \pm 3 \text{ W/m}^2\cdot\text{K}$ for the ISO conditions.

Thermography Chamber

The thermography chamber allows control and measurement of bulk air temperatures and velocity on one face of a specimen and uses an IR imager to measure the specimen. The exterior

of the thermography chamber used in the IRLab has an outer size of 1.4 m wide and 2.1 m high with a depth that can vary from 0.9 to 4.2 m (see Figure 3). The chamber is also equipped with a computer-controlled traversing system for remote and programmable motion of a point infrared thermometer or a fine wire air temperature thermocouple (Griffith 1998). Extendible bellows allow for a variable viewing distance. The IR imager was located inside the chamber and operated remotely with the aid of a motorized tilt-and-pan mount. Air circulation and conditioning equipment was located in a subfloor beneath the specimen and viewing enclosure. This design is significantly different than that of a conventional hot-box, which uses a baffle near the specimen to direct air flow and provide even thermal radiation. The IRLab chamber has an open layout, so that the infrared imager is able to "view" the specimen. Fan-induced pressure differences between the intake and output slots cause a small volume of air to be exchanged with the warm chamber. The temperature control points are located about 200 mm from the specimen plane and above it, where the entrained air would be expected to originate. The three zones of control span the width of the test section but are not physically separated. Variable-speed can be tuned to alter the amount of air mixing in the warm chamber. The fan power level is adjusted during CTS testing in an attempt to reach a target total surface film coefficient of about $8.0 \text{ W/m}^2\text{-K}$. During testing of the first specimen, the CTS, the overall surface conductance was measured at $8.0 \pm 0.4 \text{ W/m}^2\text{-K}$ for the ASHRAE conditions and 8.0 ± 0.5 for the ISO conditions.

The thermography chamber was not designed for calorimetric testing, so no serious effort has been made to reduce or eliminate heat flow through the walls or air leakage into the chamber. The chamber is also opened up at times during testing, to change positions of the imager and reference targets and to apply and remove background mirrors. Unfortunately, the surrounding laboratory space is not conditioned and can fluctuate in temperature (temperatures

were 18° to 25° C for these measurements), so periods of warm weather can have a deleterious affect on the laboratory chamber’s performance. In situations where heat gains into the chamber are too large, the chamber's gentle air-temperature-control strategy can break down; and an undesirable situation can develop where air doesn’t mix well as cool air pools in the bottom of the chamber and the subfloor becomes much colder than the other enclosure surfaces. This “stratified” condition provides bulk air that is not uniform, with temperature variations of as much as 4°C. Bulk air temperature gradients were monitored at the two locations shown in figure 3.

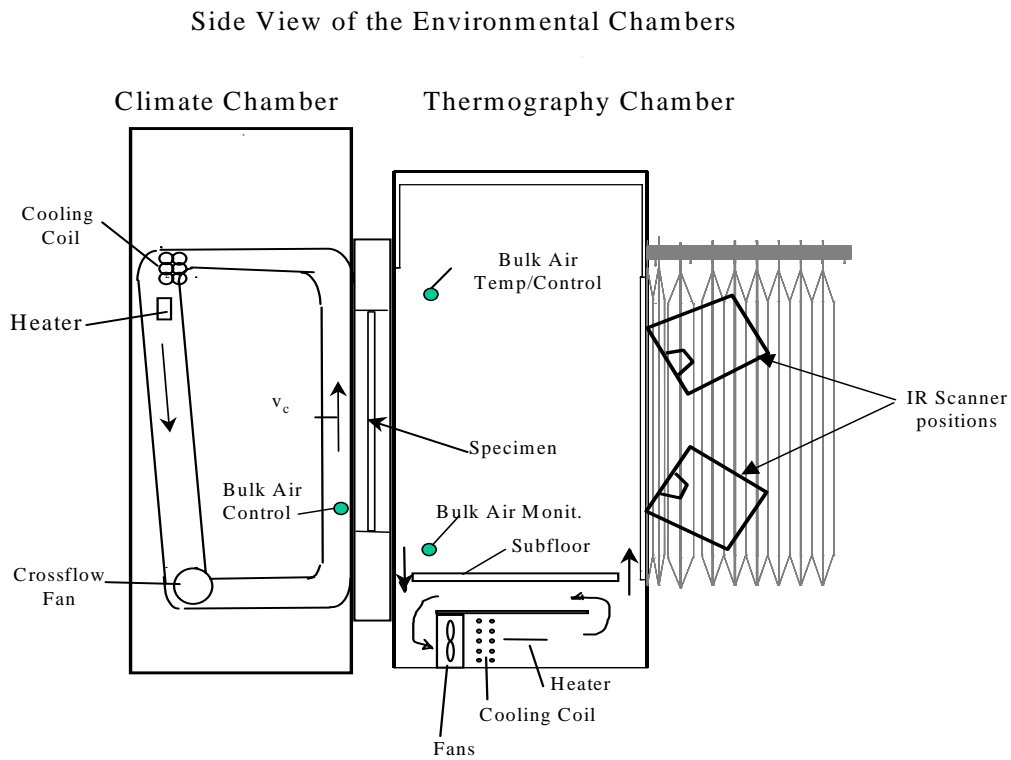


Figure 3. Schematic of Laboratory Thermal Chambers and Sensor Locations

INSTRUMENTATION

Data Acquisition

The test chambers are controlled and monitored with a computer-based data acquisition system that records bulk air temperatures, air velocities, surround panel surface temperatures, specimen surface temperatures, enclosure surface temperatures, and relative humidity. Surfaces are measured using calibrated 30-gauge type-T thermocouples. The locations of the controlling thermistor-based temperature sensors are diagrammed in Figure 3. Additional thermistors help to characterize the uniformity of bulk air in the chambers.

A separate precision thermometer system with three channels is used to calibrate sensors, to continuously verify the accuracy of bulk air temperature control during testing, and to measure the temperature of the reference target used to calibrate infrared thermographic data. This reference thermometer system measures 100- Ω platinum resistance thermometer (PRT) probes using a four-wire technique with a system accuracy of 0.02°C (0.04°F) (AC 1992). The system's calibration is traceable to the National Institute of Standards and Technology and uses the 1990 International Temperature Scale.

Infrared Radiometers

A scanning IR imaging radiometer (scanner) was used to measure surface temperatures of the specimens (BSI 1993). The IR scanner used here is a long-wave (8 to 12- μm), high-speed imager that uses mercury/cadmium/telluride detectors to measure radiosity of the test specimen and

reference targets. The IR scanner is a computerized system that can capture and average frames of data and export image-based data sets.

A point IR thermometer was also used to measure surface temperatures with the aid of a traversing system (RC 1997). The single point thermometer is a close-focus unit designed to measure a spot of about 3 mm at a distance of 75 mm from the surface. The sensor and measurement system was calibrated in our laboratory during initial setup with the help of an extended-area blackbody (CIS 1992).

Reference Target

The reference emitter used in these experiments is a custom device based on a temperature-controlled liquid system. A fluid channel was machined into a copper block, leaving a 13-mm-thick solid portion directly underneath the reference surface. A bore reaches to the center of the solid portion that accommodates a PRT probe. A 3-mm-thick sample of window glass was mounted on part of the reference emitter using a heat sink compound. The other part was painted. The temperature-controlled liquid is supplied by a recirculating bath with a built-in microprocessor controller that is stable over time to within 0.01°C. The back, sides, and fluid lines of the reference emitter are insulated and designed and placed so that its presence interferes minimally with air temperature and flow results. The reference surface temperature for the glass was adjusted from substrate measurements using the PRT to account for heat flow and temperature gradients through the glass. Two infrared mirrors are also mounted on the reference emitter for quantifying background thermal radiation. One mirror is aluminized polyester film

and the other is gold-coated aluminum with a surface shaped to provide a diffusely reflecting infrared surface.

MEASUREMENT PROCEDURES

View Arrangements

Infrared tests for each specimen were divided into four separate measurement cycles: sill region, bottom half, top half, and header region. In order to obtain a view of the horizontal surfaces that are perpendicular to the glazing in the sill and head regions of the specimen, measurements used close-up views taken at about 45° angles. The imager was mounted in a high position for imaging the sill region and a low position for imaging the header as shown in Figure 3. The bottom half of the window was imaged from the upper position by changing the tilt, and the top half of the window glazing was imaged from the lower position. Figure 4 diagrams these four views.

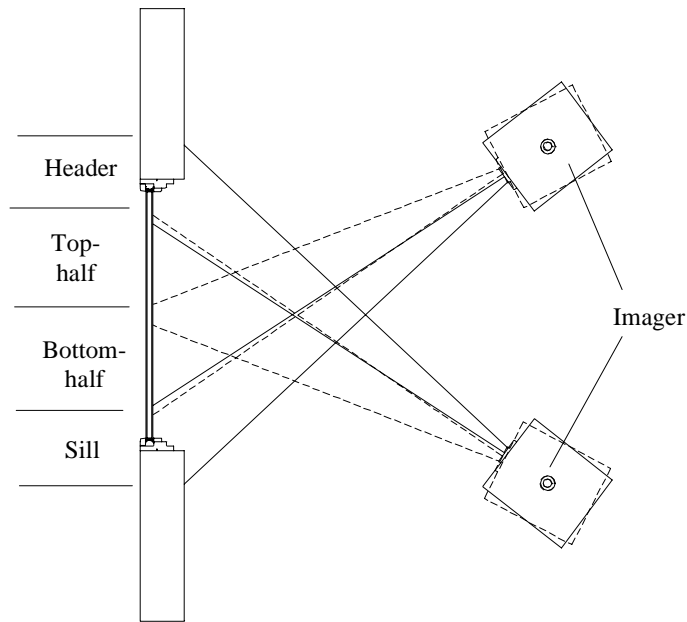


Figure 4. Schematic of Four Image Views

Each thermal image was composed so that a reference emitter with multiple targets for calibrating the IR data was included in the view. The addition of external referencing targets allows improving the absolute accuracy of the temperature measurements. During each measurement, the reference emitter was situated near the specimen being measured and within the field of view of the IR imager. The reference emitter was kept reasonably in focus while the imager was focused on the test specimen.

In contrast to IR thermography for flat surfaces, complex background thermography requires additional steps to gather background radiation levels. After the first set of uncorrected IR data (from both the scanner and the traversing point thermometer) were obtained, data were gathered for the effective temperature of the background at each location by temporarily applying background mirrors (aluminized polyester film) to the specimen in two stages. Mirrors were first

applied to vertical surfaces on the specimen. After the mirror reflections were measured, these mirrors were removed, and new mirrors were applied to the horizontal surfaces. The scanner viewing angle, the point thermometer's traversing path, and the specimen geometry remained the same for each part of the cycle. Thus, for each view, three sets of images or data were collected, the unmodified surface, the background levels for vertical surfaces, and the background levels for horizontal surfaces.

Point measurements

The traversing system is programmed to move the sensor, pause it at a measurement location, and trigger the data-acquisition system to record readings. Figure 5 diagrams the movement of the single-point IR thermometer along the sill of one of the wood casements. No external referencing of the point thermometer was performed because there was not enough travel in the system to view the reference emitter target.

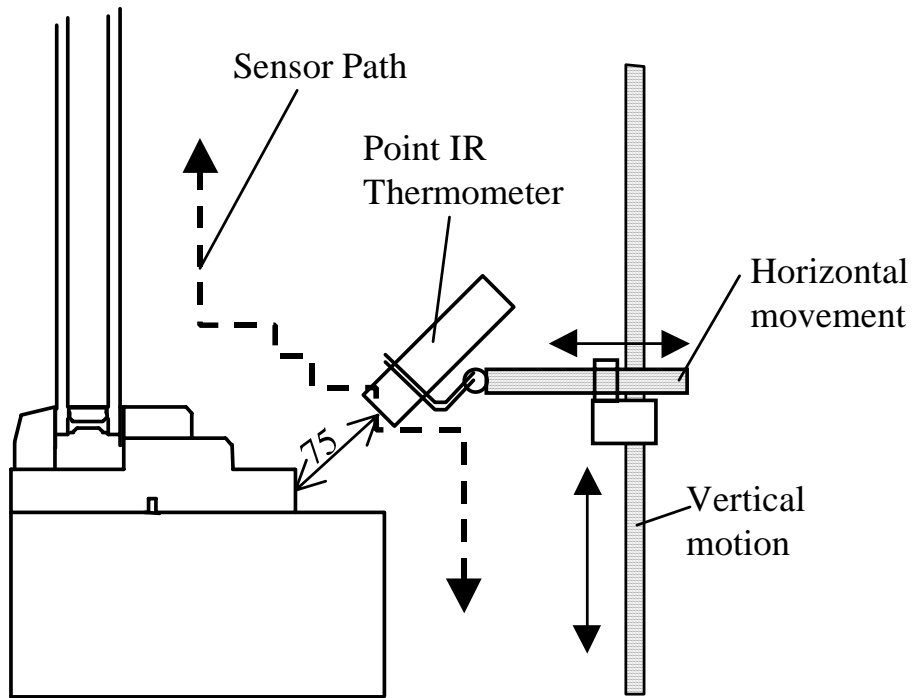


Figure 5. Schematic of Point IR Thermometer Traversing Technique

DATA ANALYSIS

Surface Emittance

Emittance describes the ability of a body to emit radiation. We need to figure out the appropriate emittance value for the particular material in each window specimen and for the IR imager being used. Emittance is defined as the ratio of the rate of radiant emission of the body, as a consequence of temperature only, to the corresponding emission of a perfect emitter (blackbody) at the same temperature. Although emittance refers to a basic material property that, in principal has one true value, it is used here in a slightly different fashion: the appropriate emittance value to use for quantitative infrared thermography is scaled by the wavelength-dependent response of

the detector used in the radiometer. This emittance value may differ from literature values and may vary among different radiometers. Thus, in our procedures, the appropriate values to use for emittance of the various materials on a specimen's surface are first measured in a separate experiment that compares the specimen's emittance to the emittance of a known material. Thin specimens of both the known material and the unknown sample material are mounted in good thermal contact to an isothermal, temperature-controlled plate and brought to the same surface temperature. The temperature is set to 20°C above the background temperature to insure high contrast between the radiosity from the specimens and the radiation from the background. The infrared imager is set to emittance 1.0 to turn off any background radiation compensation. Both specimens are imaged simultaneously. Readings are averaged over both time and space for the equivalent blackbody temperature of the unknown sample, $T_{e=1,\text{smp}}$, and the equivalent blackbody temperature of the known reference material, $T_{e=1,\text{ref}}$. Background radiation equivalent blackbody temperature, T_{back} , is quantified using a background mirror. Caution is exercised to provide a very uniform background, which is verified by imaging the background mirror. The emittance of the sample material, e_{smp} , is then calculated from the emittance of the known material, e_{ref} , using equation 1. Temperature units are Kelvin. Several measurements are made and then averaged.

$$e_{\text{smp}} = \frac{\left(T_{e=1,\text{smp}}^4 - T_{\text{back}}^4 \right)}{\left(T_{e=1,\text{ref}}^4 - T_{\text{back}}^4 \right)} e_{\text{ref}} \quad (1)$$

Table 2. Emittance Values for Mercury/Cadmium/Telluride Infrared Measurements

Material	Emittance
Glass	0.86
Wood	0.90
Vinyl tape	0.90
Paint	0.90

Infrared Temperature Calculations

In order to obtain quantitative surface temperatures, the raw thermographic data were first extracted from the thermography software so they could be processed in a separate mathematical program. The thermography software was used to extract data from the thermal image and them in appropriate arrays of text values synchronized with spatial coordinates. The result for temperature at each data point was calculated with the correct emittance and a location-specific background level. The calculated IR temperature for the reference emitter was compared to direct contact measurements, and deviations were used to scale the rest of the IR data. Four separate data sets were merged together to combine data from different close-up views.

Equation 2 shows an expression for calculating a surface temperature, T_{IR} , from the total thermal radiation represented by the variable $T_{e=1}$, the emittance of the surface, e_{surf} , and the background radiation level represented by the variable T_{back} . $T_{e=1}$ is an equivalent blackbody temperature for the surface being measured. T_{back} is the equivalent blackbody temperature for the background

thermal radiation level as measured at each location with the aid of an applied mirror. Values for both $T_{e=1}$ and T_{back} are obtained from the thermography system by setting emissivity to unity.

$$T_{IR} = \left(\frac{(T_{e=1}^4 - (1 - e_{surf})T_{back}^4)}{e_{surf}} \right)^{1/4} \quad (2)$$

Equation 2 is used to determine both the apparent reference emitter temperature, $T_{IR,Ref}$, (as measured by IR imaging) and the apparent sample surface temperature, $T_{IR,smpl}$. We used both glass and painted reference targets to obtain $T_{IR,Ref}$ for each material to reference sections of the specimen with the same the same emittance. The difference between $T_{IR,Ref}$ and the direct contact measured value, $T_{DC,Ref}$, was applied to correct $T_{IR,smpl}$ and to arrive at the final IR surface temperature result, T , as shown in Equation 3. This correction was made for each temperature datum and for each IR image, to produce arrays of temperature values.

$$T = T_{IR,smpl} - (T_{IR,Ref} - T_{DC,Ref}) \quad (3)$$

Final data sets merge spatial location coordinates with temperature values. The real distances between location markers on the specimen were measured, and a coordinate system was used to create temperature/location data pairs. The temperatures were distributed linearly. Temperature data were then made into a function of x and y spatial coordinates, mapped to the coordinate system being used. The data sets have the form (L, T) where L is the accumulated distance along the surface.

Infrared Temperature Uncertainty

Quantitative thermography requires a careful estimate of uncertainty in the data. A previous publication by the authors discusses in detail the origination of the following equations used to propagate uncertainty (Türler 1997). Errors in e_{surf} should be treated as a source of nondefinable

systematic uncertainty, δe_{surf} , and may be analyzed by propagating uncertainty in Equation 1. Errors in $T_{e=1}$ and T_{back} lead to random uncertainties, $\delta T_{e=1}$ and δT_{back} . $\delta T_{e=1}$ and δT_{back} are usually closely related to equipment specification for Noise Equivalent Temperature Difference (NETD). To analyze error propagation in Equation 2, we calculate the sum of the squares of partial differentials of Equation 2 with respect to variables $T_{e=1}$, T_{back} , and e_{surf} , which leads to one possible solution, shown in Equation 4. The uncertainty in T_{IR} , δT_{IR} , is then calculated using Equation 4.

$$\delta T_{\text{IR}} = \frac{1}{4} \left(\frac{T_{e=1}^4}{e_{\text{surf}}} + T_{\text{back}}^4 - \frac{T_{\text{back}}^4}{e_{\text{surf}}} \right)^{-\frac{3}{4}} \left(\sqrt{\left(4 \frac{\delta T_{e=1}}{e_{\text{surf}}} T_{e=1}^3 \right)^2 + \left(4 T_{\text{back}}^3 \delta T_{\text{back}} - 4 \frac{\delta T_{\text{back}}}{e_{\text{surf}}} T_{\text{back}}^3 \right)^2 + \left(\frac{\delta e_{\text{surf}}}{e_{\text{surf}}^2} T_{\text{back}}^4 - \frac{\delta e_{\text{surf}}}{e_{\text{surf}}^2} T_{e=1}^4 \right)^2} \right) \quad (4)$$

The total uncertainty in the measured surface temperature, δT , is obtained from Equation 5. Values for both $\delta T_{\text{IR,smpl}}$ and $\delta T_{\text{IR,Ref}}$ are obtained using Equation 4. The uncertainty in the direct contact measurement of the reference emitter surface temperature, $\delta T_{\text{DC,Ref}}$, is determined from the overall system accuracy of the direct contact sensor combined with any errors associated with adjustments that correct for gradients in the surface material. The uncertainty arising from variations across the field of view, δT_{FOV} , is determined from the magnitude of deviations in heavily averaged data for an isothermal plate that fills the section of the field of view being used.

$$\delta T = \delta T_{\text{IR,smpl}} + \delta T_{\text{IR,Ref}} + \delta T_{\text{DC,Ref}} + \delta T_{\text{FOV}} \quad (5)$$

Environmental Uncertainty

In addition to the uncertainty δT in measuring the true surface temperature, there is also uncertainty in how well the chambers can create steady-state conditions with constant,

repeatable, true temperatures resulting on a particular specimen. The situation introduced above, where the surrounding laboratory space becomes too warm, can alter the environmental conditions to which the specimen is exposed, creating a significant shift in the true temperatures. There could also be transient convective phenomena so that steady-state, constant real temperatures do not even exist. In order to quantify the errors associated with such a shift, we analyzed results for direct contact surface temperature sensors. Recall that, for some tests, thermocouples were mounted on specimen surfaces at four locations. After the specimen undergoes an extended period of conditioning and approaches steady-state (with chambers at setpoint), the fluctuations in surface temperatures were used to assess the magnitude of shifts in the real temperature resulting from environmental conditions, δT_{Envi} . Experience in operating the chambers shows that, laboratory space overheating problems do not occur during the night. These nighttime data from test periods with good temperature stability and uniform bulk air temperatures are baseline conditions to judge when the chambers are performing well. Results for the direct contact thermocouple measurements were taken from such baseline periods of operation. Data from periods during which the chamber was not performing as well were analyzed to determine how much δT_{Envi} could be shifting the temperature results from what they would be if environmental conditions were ideal. The uncertainty of the calibrated thermocouple measurements was estimated at $\pm 0.2^\circ\text{C}$. This uncertainty was added to δT_{Envi} to arrive at overall estimates for error in the data.

RESULTS

Environmental Conditions

Table 3 shows the results from the CTS testing, which help characterize the chamber conditions during the baseline, or best, periods of operation. We directed our efforts toward achieving a total warm-side film coefficient of $8 \text{ W/m}^2\cdot\text{K}$, a minimal modification of both ASHRAE and ISO standard conditions. We found that fan power in the warm box needed to be higher for the ISO conditions to obtain similar total surface heat-transfer rates to those for the ASHRAE conditions.

Table 3. Results from Baseline CTS Measurements for Total Surface Heat-Transfer Rates

		ASHRAE Conditions	ISO Conditions
WARM SIDE	Air Temp. (°C)	21.1 ± 0.1	20.0 ± 0.1
	Total Film Coef. ($\text{W/m}^2\cdot\text{K}$)	8.0 ± 0.4	8.0 ± 0.5
COLD SIDE	Air Temp. (°C)	-17.78 ± 0.05	0.0 ± 0.05
	Total Film Coef. ($\text{W/m}^2\cdot\text{K}$)	30 ± 2	24 ± 3

Table 4 summarizes some of the important measures of environmental conditions at the time of each test. These data are presented to show the fluctuations in conditions to which the specimens were exposed.

TABLE 4. Environmental Conditions During Specimen Measurements

Test ID	Portion of Test (IR View)	Cold-side Velocity (m/s)	Warm-side Temp. @ Control (°C)	Surrounding Laboratory Temp. (°C)	Bulk Air Temp Vert. Gradient (°C)	Subfloor Enclosure Surf. Temp. (°C)
CTS_ISO	Baseline	2.0	20.02	19.4	0.1	19.7
	Sill	1.8	19.9	23.2	0.8	18.7
	Bottom half	2.8	20.1	22.7	0.9	18.6
	Top half	2.0	20.1	20.3	0.1	19.0
	Header	1.9	20.0	22.3	0.4	19.0
CTS_ASHRAE	Baseline	2.4	21.04	22.0	0.9	21.0
	Sill	2.1	21.1	18.5	0.7	21.9
	Bottom half	2.3	21.3	23.8	1.6	19.6
	Top half	1.9	21.3	22.9	2.0	19.3
	Header	2.0	21.3	22.2	1.3	19.3
Clear_ISO	Baseline	2.8	20.04	21.0	0.4	19.6
	Sill	2.8	20.05	21.3	0.4	19.6
	Bottom half	2.7	20.00	19.9	0.5	19.7
	Top half	2.5	20.06	23.3	0.7	18.7
	Header	2.5	20.05	22.8	0.4	19.6
Clear_ASHRAE	Baseline	3.7	21.21	17.9	1.4	21.7
	Sill	3.6	21.19	22.2	1.8	20.4
	Bottom half	3.6	21.16	21.9	2.0	20.0
	Top half	3.4	21.22	22.7	1.6	20.7
	Header	3.4	21.27	20.6	1.4	21.4
Low-E_ISO	Baseline	2.8	20.02	21.7	0.2	20.1
	Sill	2.8	20.08	24.9	3.9	15.9
	Bottom half	2.8	20.10	24.3	0.4	19.0
	Top half	2.6	20.05	22.3	0.5	19.8
	Header	2.6	20.17	22.8	0.7	19.5
Low-E_ASHRAE	Baseline	3.7	20.07	21.8	1.2	21.3
	Sill	3.3	21.09	20.7	1.5	20.6
	Bottom half	3.2	21.00	22.6	1.5	20.3
	Top half	3.5	21.21	24.8	1.6	19.8
	Header	3.7	21.21	22.7	1.0	21.0

Surface Temperatures

Figures 6 through 11 show the results for surface temperature. Each plot presents the measurements from the IR scanner, the traversing point IR thermometer, and any surface temperatures measured using direct-contact thermocouples. Error bars plotted for the direct-contact thermocouples include the estimated error in the thermocouple measurement of $\pm 0.2^{\circ}\text{C}$ and the observed fluctuations in these measurements that are assumed to be a result of varying environmental conditions. The direct contact measurements from the CTS's thermocouples fluctuated less than those of the thermocouples applied with tape. The total uncertainty in the IR imager measurements was estimated to be $\pm 0.5^{\circ}\text{C}$. No estimate of uncertainty was made for the IR point measurements.

DISCUSSION

The data for surface temperatures are inconsistent. In most cases, the direct-contact thermocouple data disagree with the IR data even when we take into account the possibility of shifts in the true temperature as a result of environmental conditions that diverged from baseline. The colder the specimen, the worse the disagreement. The direct-contact data from the CTS's embedded thermocouples agree with the IR data better than the direct-contact data from tape-applied thermocouple wires. This suggests that the error may be associated with projecting thermocouple surface mounting methods. Another likely cause of inconsistencies is a recently identified problem with the data-acquisition system that measures the thermocouples. The two-tiered signal multiplexer does not provide perfectly independent signal switching. As a result, adjacent channels in the multiplex switching scheme can influence each other. The effect is subtle and difficult to quantify when there is a small difference between the physical

temperatures being measured; however, experience with this equipment since these measurements were originally taken suggests that the error could easily be on the order of the disagreement between the surface thermocouple and IR data reported here. The data-acquisition hardware for thermocouples is being replaced to eliminate this source of error in future measurements. Additional possible sources of systematic error that have been investigated but not dismissed include: (1) mistakes may have been made in computer programming routines used to process IR temperature data, (2) the PRT thermometer system may not have been functioning properly, (3) linearity in the calibration of the IR imager may have been worse than expected, (4) uniformity across the field of view of the IR imager may have been worse than expected, and/or (5) the wavelength response of the IR imager may have been lower than expected, resulting in measuring IR that was transmitted through the glass. We were unable to repeat measurements or fully investigate the cause of the inconsistencies observed in the data because the measurements were part of a round robin, and data post-processing did not occur until well after the experimental specimens had been sent to another laboratory.

The sill view of the low-E window under ISO conditions was taken during a period when the thermography chamber was not performing well. Because the chamber is not sufficiently insulated or guarded from ambient conditions, hot weather has been observed to cause thermal stratification within the chamber that the gentle mixing of controlled air cannot overcome. When operating under these conditions, the vertical bulk air temperature gradient can be as high as 4°C (see Table 4, low-E ISO sill). This condition is responsible for the discontinuity of IR temperatures observed in Figure 10, where the data collected for the sill meets that of the bottom

half of the glazing. The sill temperatures are uniformly low because of the bulk air stratification of colder air toward the bottom of the chamber.

Although the measured data are not internally consistent in their absolute accuracy, a number of interesting observations result from studying the relative distribution of surface temperatures on windows. It is well known that window glazings under such conditions have a temperature gradient in the vertical direction; the usual explanation is that this gradient is a result of convective flows inside the glazing gap. The data for the CTS, however, show temperature gradients at the center of glass that are comparable to those of the glazing even though the CTS has closed-cell foam rather than an air gap. These data show that localized convective effects *outside* the window gap are very important to an accurate prediction of surface temperatures. Controlled, bulk temperature, air first encounters the specimen at the head and falls as it cools. Lower portions of the specimen are therefore exposed to heat exchange with progressively colder air resulting in a surface temperature gradient, which is colder at the sill, as observed.

The point thermometer did a reasonably good job of capturing the shape of the temperature distribution curves, but the instrument does not appear to have been calibrated well enough to provide sufficiently accurate data. This experiment was a first attempt to gather these data using a point thermometer; this method shows promise and warrants further research. A helpful addition to the experimental protocol would be a technique for referencing infrared measurement in a fashion similar to that used for the scanner measurements. There appears to be an issue with off-angle measurements because results for measurements taken with the instrument oriented at a

45° angle were not consistent with results for measurements taken perpendicular to the specimen surface.

Although the data are not consistent, the combination of non-contact IR scanner measurements and direct-contact thermocouple measurement does offer an opportunity to investigate the practice of applying thermocouple wires to surfaces using adhesive tape and any local changes in temperature that result from this method. The bulge of wire and tape for the thermocouple sticks up off the surface and therefore is subject to different convection conditions than the unmodified specimen surface. A localized change in surface emittance also alters thermal radiation conditions. For center-of-glass measurements, the IR scanner data show local maxima at the thermocouple wire; these maxima are 0.25 to 1.0 °C higher than the surrounding surfaces. The direct-contact measurements from the CTS thermocouples agreed well with those from the tape-applied thermocouple wires for the ISO conditions but not for the ASHRAE conditions. This suggests a need to further characterize the precision and bias of surface-temperature measurements using direct-contact wires.

CONCLUSIONS

Experimental data were generated using infrared thermography to characterize the distribution of surface temperatures on windows under heating conditions in laboratory chambers. This was done for three specimens: a Calibrated Transfer Standard, a clear wood casement, and a low-E wood casement. The data plotted in Figures 6 through 11 are intended to assist in efforts to validate and develop computer simulation tools that predict surface temperatures of window

assemblies. Direct-contact thermocouple wires were also attached to the specimens using vinyl tape. In most cases, the direct-contact thermocouple data did not agree well with the IR data. The reasons for the inconsistency have not been determined.

Although the intent of laboratory test chambers is to provide repeatable and stable environmental conditions, the chambers did not maintain the desired bulk air temperature set point during periods of hot weather. The resulting uncertainty in temperatures was as much as $-2/+1^{\circ}\text{C}$. IR data for the sill of the low-E window under ISO conditions were collected during a period when the chamber was not performing reliably.

The experimental measurements conducted here require careful procedures and detailed post processing, which make it generally impractical to perform measurements using these techniques on a routine basis.

ACKNOWLEDGMENTS

The authors thank Nan Wishner for her assistance in editing this paper. This work was supported by the Assistant Secretary for Energy Efficiency and Renewable Energy, Office of Building Technology, State and Community Programs, Office of Building Systems of the U.S. Department of Energy under Contract No. DE-AC03-76SF00098.

REFERENCES

AC. 1992. Operation and maintenance Instructions: A1011 Precision RTD Thermometer. Azonix Document F19-100257. Billerica, MA.: Azonix Corporation.

ASTM. 1995. ASTM C 1199, Standard test method for measuring the steady state thermal transmittance of fenestration systems using hot box methods. *Annual Book of ASTM Standards*, vol. 04.06: 671-682. Philadelphia, PA: American Society for Testing Materials.

BSI. 1993. The BSI TIP Thermal Image Processor Operator's Manual. Walnut Creek, CA: Bales Scientific Inc.

CIS. 1992. SR 80 extended area infrared radiation source operation manual. Agoura Hills, CA.: CI Systems, Inc.

de Abreu, P., Fraser, R.A., Sullivan, H.F. and Wright, J.L., 1996. A study of insulated glazing unit surface temperature profiles using two-dimensional computer simulation. *ASHRAE Transactions* Vol. 102(2).

Elmahdy, H. 1996. Surface temperature measurement of insulated glass units using infrared thermography. *ASHRAE Transactions* Vol. 102(2).

Griffith, B.T., D. Türlér, and D. Arasteh. 1996. Surface temperatures of insulated glazing units: infrared thermography laboratory measurements. *ASHRAE Transactions* Vol. 102(2).

Griffith, B.T., D. Turler, H. Goudey, and D. Arasteh. 1998. Experimental techniques for measuring temperature and velocity fields to improve the use and validation of building heat transfer models. *Thermal Performance of the Exterior Envelopes of Buildings VII*. Atlanta, GA: American Society of Heating, Refrigerating, and Air-Conditioning Engineers, Inc.

RC. 1997. Thermalert TX™ Series Operator's Manual. Santa Cruz, CA: Raytek Corporation.

Sullivan, H.F., Wright, J.L. and Fraser, R.A. 1996. Overview of a project to determine the surface temperatures of insulated glazing units: thermographic measurement and two-dimensional simulation. *ASHRAE Transactions* Vol. 102(2).

Turler, D., B.T. Griffith, and D. Arasteh. 1997. Laboratory procedures for using infrared thermography to validate heat transfer models. *Insulation materials: Testing and Applications: Third Volume ASTM STP 1320*. R.S Graves and R.R. Zarr, ed. Philadelphia, PA: American Society for Testing and Materials.

Zhao, Y., D. Curcija, and W.P. Goss. 1996. Condensation resistance validation project - Detailed computer simulations using finite element methods. *ASHRAE Transactions* Vol. 102(2).

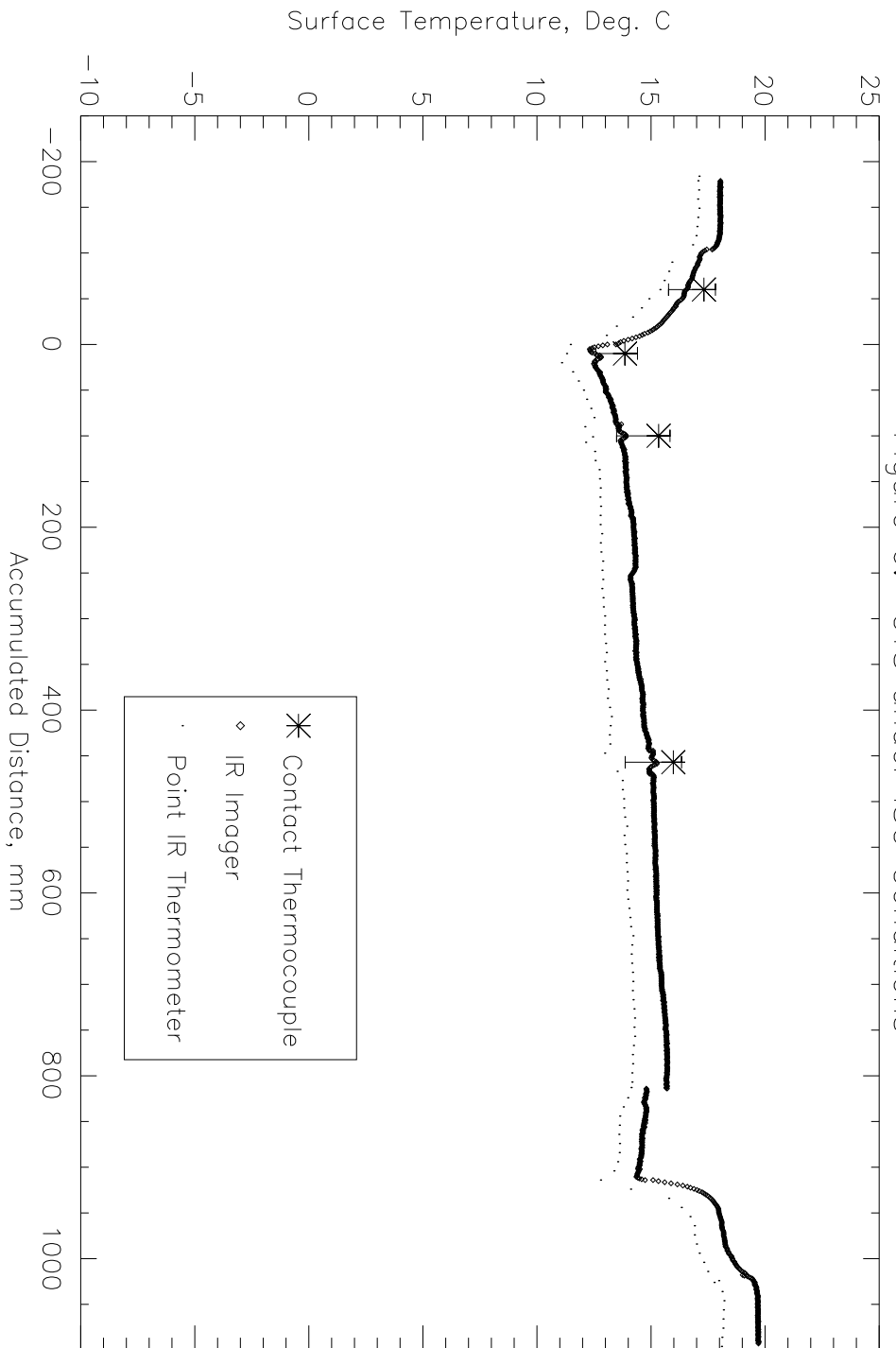


Figure 6. CTS under ISO Conditions

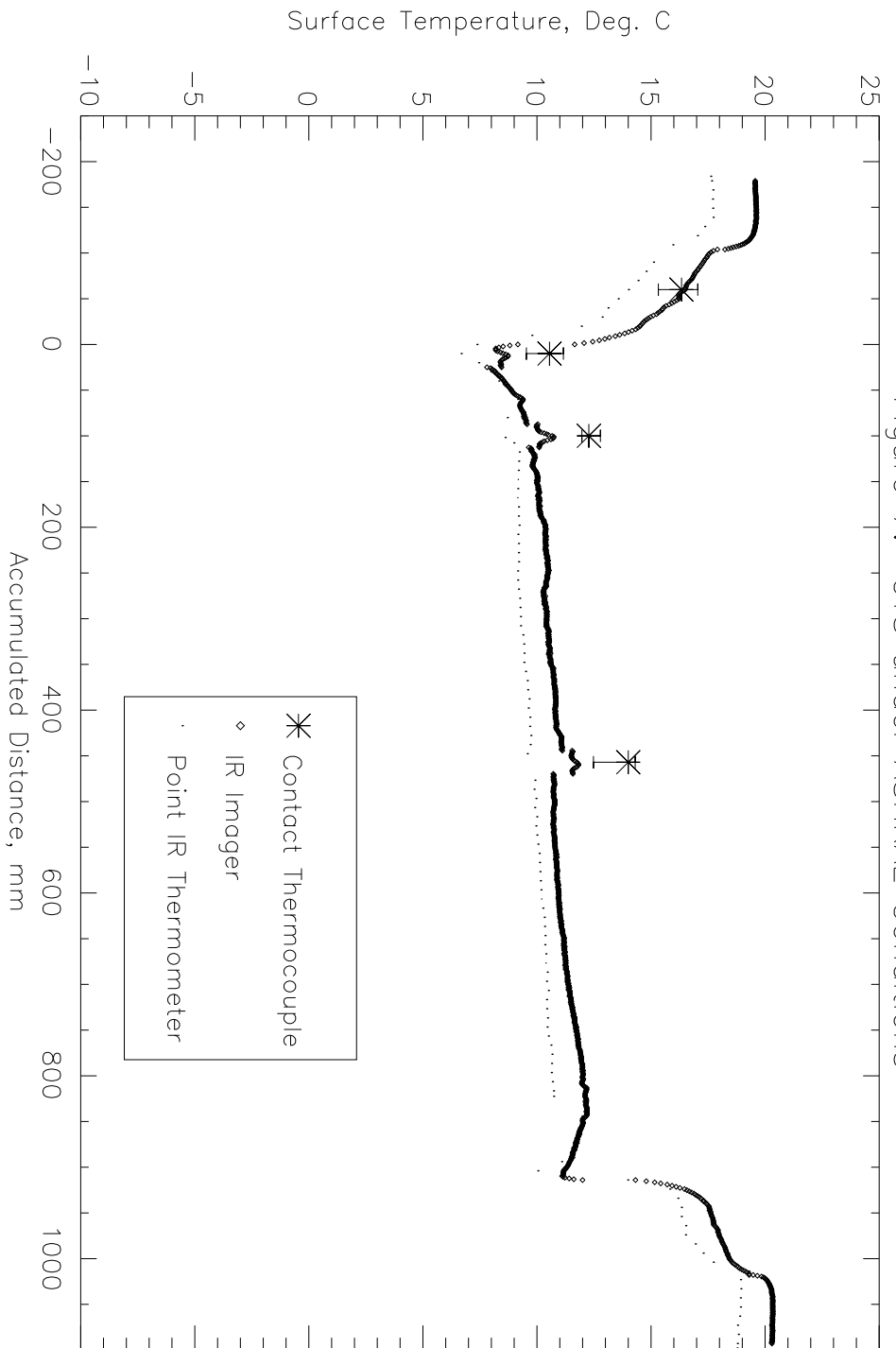


Figure 7. CTS under ASHRAE Conditions

Figure 8. Clear Wood Casement under ISO Conditions

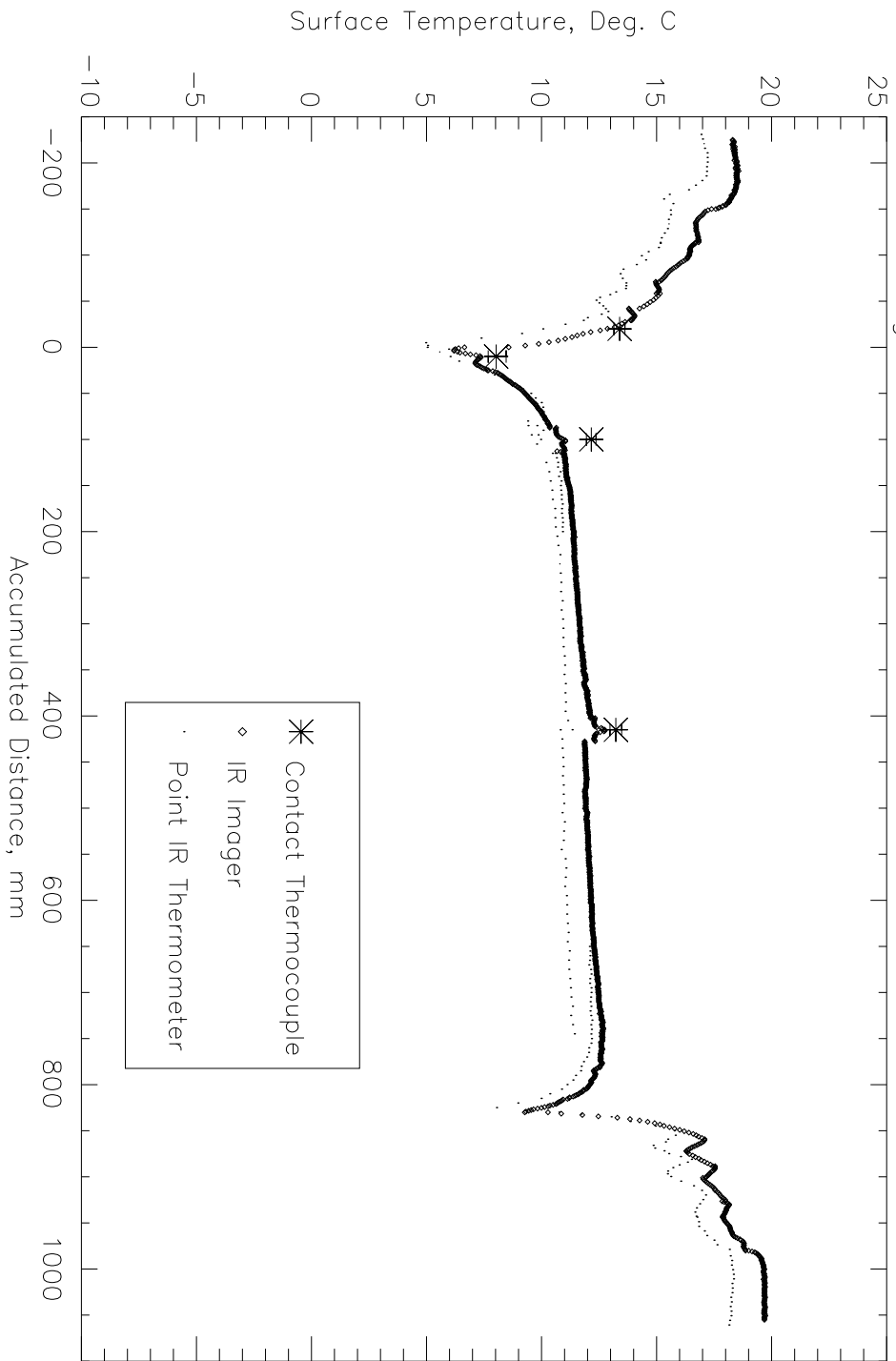


Figure 9. Clear Wood Casement under ASHRAE Conditions

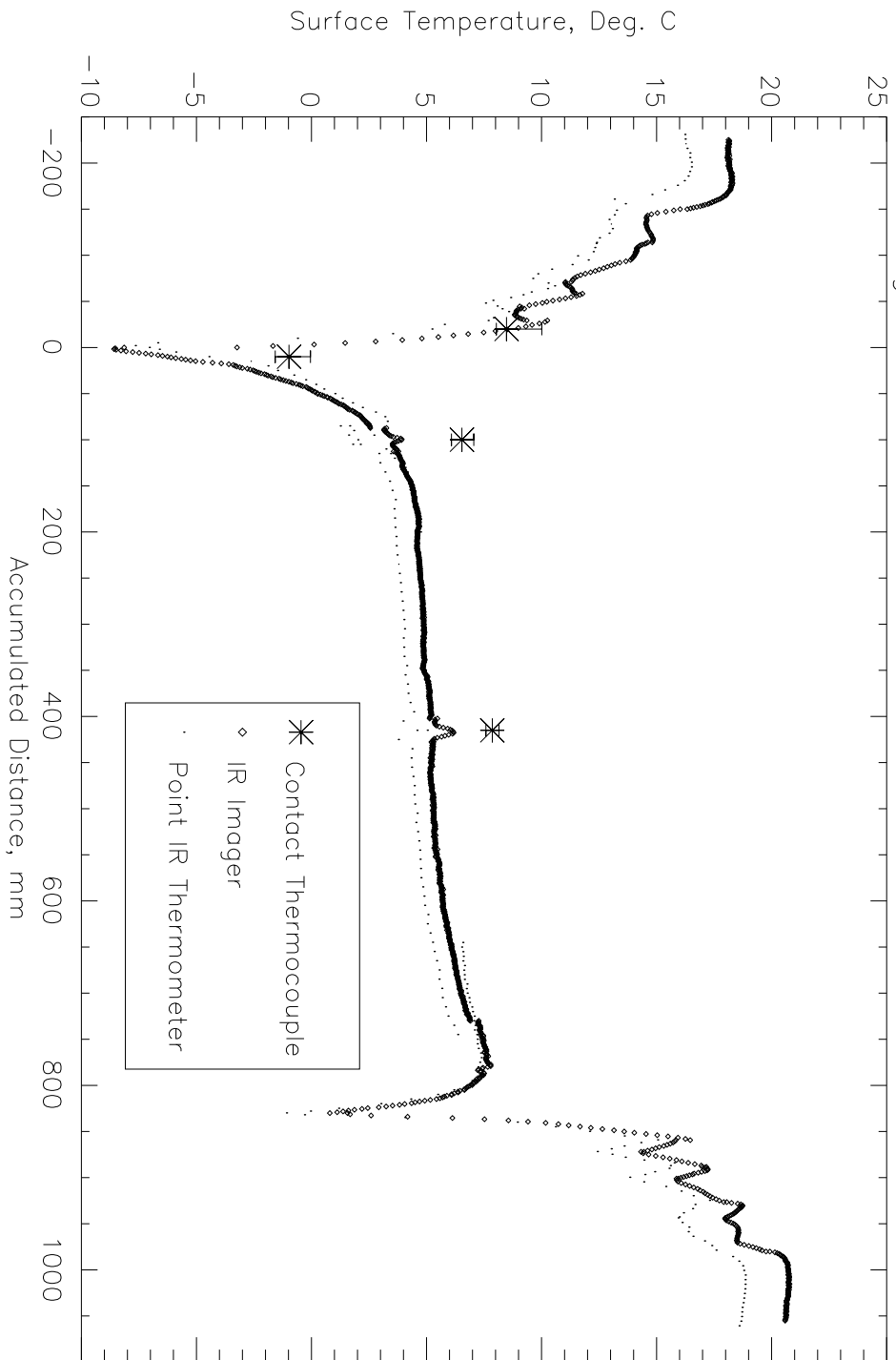


Figure 10. Low-E Wood Casement under ISO Conditions

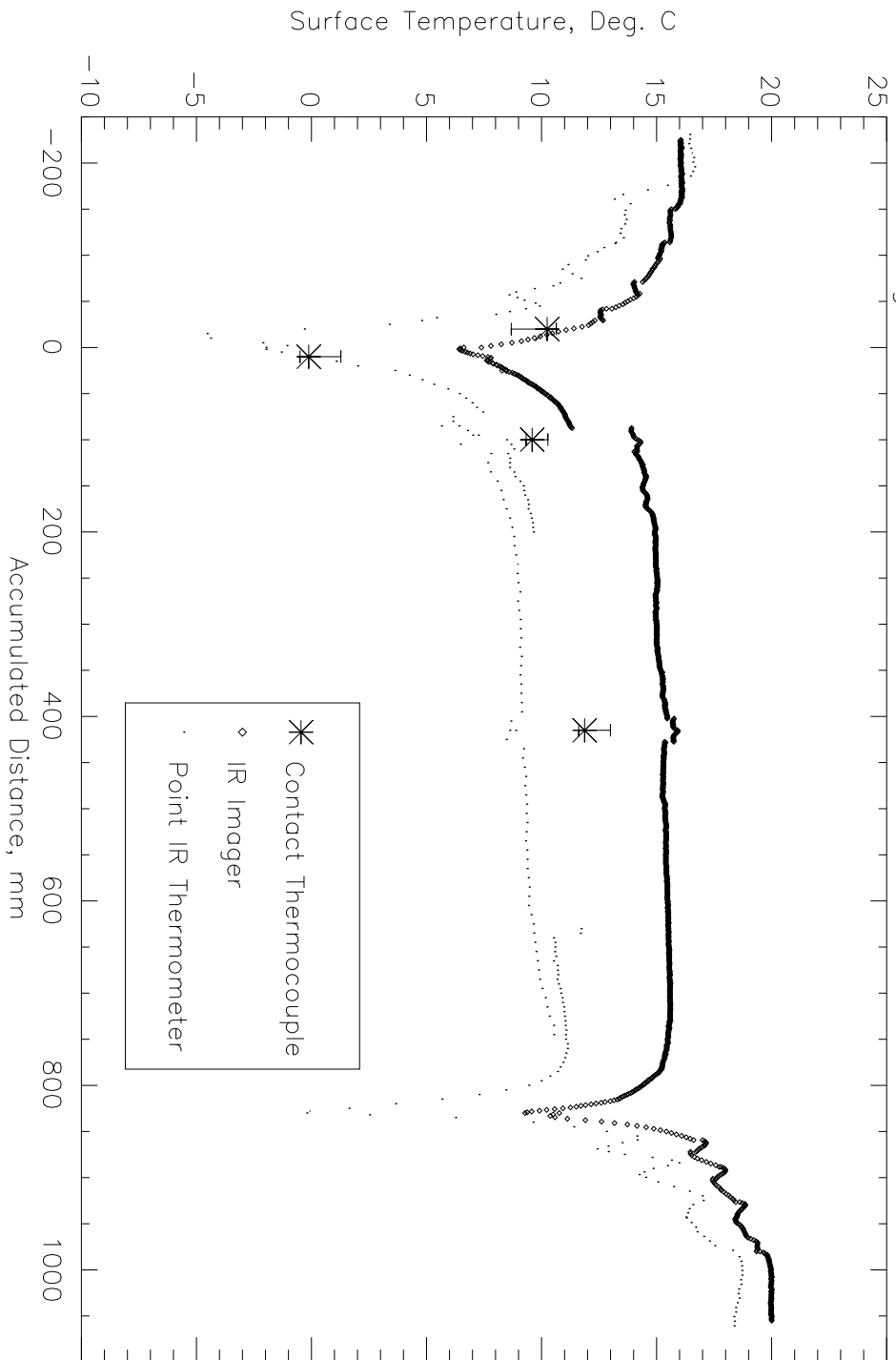


Figure 11. Low-E Wood Casement under ASHRAE Conditions

